MBI Savunma ve Alan Tarama Teknolojileri Sanayi A.Ş.

MTD-3 TEST REPORTS

MBI Savunma ve Alanı Arama Teknolojileri A.Ş
(Test Facilities)

TESTING PROCEDURE AND EXPERIMENTAL RESULTS

OF MINE DETECTOR MTD-3

1. INTRODUCTION

MTD-3 Mine Detector (*Capable to Measure Shape or Explosive Content in Addition to Metal Content*) is a subsurface sensing device which has pulse (PI) and GPR modes.

Generic view of the MTD-3 is given in Figure-1. Main processing unit communicates with the sensor controller unit and receives the acquired sensor data and then processes the data to perform detection, identification and data visualization if it is required. Main processing unit performs all high level processes such as driving of user interface, running of detection and identification software.

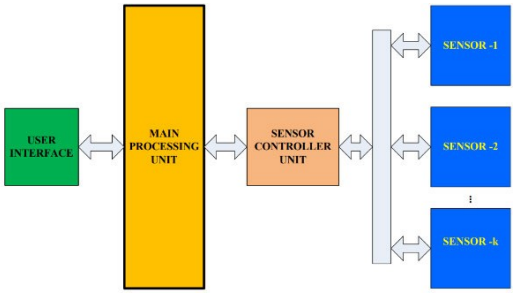

Fig. 1: Generic view of MTD-3 Mine Detector

Fig. 2: General view of Mine Detector MTD-3

MTD-3 has been currently used for detection and identification of both metallic and non-metallic buried objects. The performance of the MTD-3 exactly depends on a proper design of antennas and UWB transmitter/receiver configurations. The antennas have high directivity gain, narrow beam, low side lobe and low input reflection levels over operational frequency bands to attain a largest dynamic range, focused illumination area, reduced ringing and uniformly shaped impulse radiation.

The control and data flow diagram of MTD-3 is given in Figure-3. The Main Processing Unit (PowerPC module) meets high level computational requirements of the system. Linux Kernel based simple operating system runs over the module. The graphical user interface of the system was developed using embedded QT environment. In order to increase shifting speed of the displayed image and quality, graphical performance boosting methods were developed. Sensor Control and Synchronization Unit (FPGA hardware) collects all data of sensors with proper timings. The collected sensor data is transferred to the Main Processing Unit by means of a special data bus. There is an Ethernet port to send out all the received data to the eternal data storage if there is a connected device, is also helpful for real-time data transfer and software debug processes. Additionally, this utility can be used for online help to the operator during operation. When detection is occurred in one of the sensors, modulated sounds are created and detection functions are presented on display, which are proportional with detection strengths of each sensor(Fig.3).

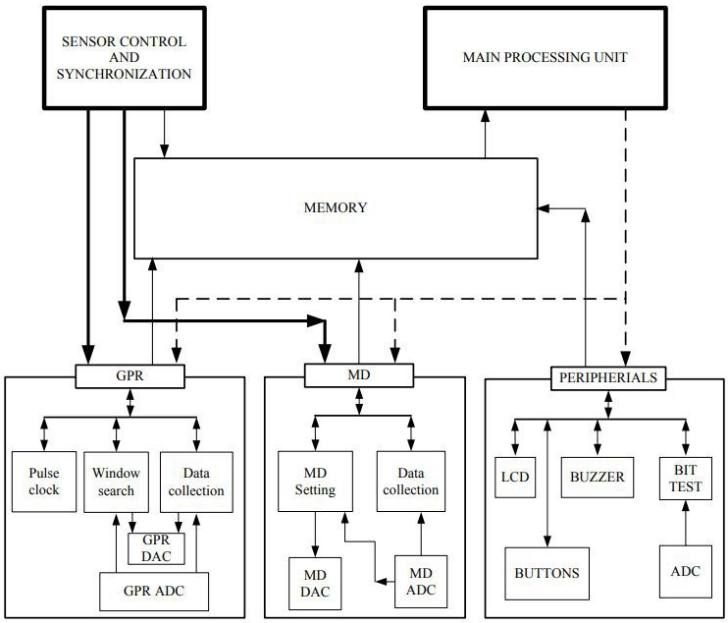

Fig. 3: Control and data flow diagram of dual sensor mine detector MTD-3

The experimental data are collected for different buried objects in three soil conditions. Nevertheless, in this study, the experimental results are given only for a surrogate TS50 mine and a metal disk due to the lack of space. The various scenarios in experiments have been analyzed with ROC curves of the proposed MTD-3 Mine Detector (Figure 4).

2. *EXPERIMENTAL SETUP AND DETECTION ALGORITHM*

In MTD-3 test study, we use N = 240 A-scans to construct B-scan data. Each A-scan data contains L = 256 samples. We assume that detection step is appropriately handled. The sensor data for the detected objects are first divided into three groups according to their metal density function, using Metal Detector (MD). Within each group, features are extracted from MTD-3 responses, and landmine/clutter discrimination is achieved using a k-NN classifier.

In order to analyze performance of MTD-3 GPR pulses, a set of measurements has been carried out at MBI Savunma ve Alanı Arama Teknolojileri A.Ş. test laboratory located in Gebze - Istanbul.

In the measurements, the durations of the pulser circuits is 650 ps. The pulse circuits is equally constructed at 256 sampling points. The Vring/Vmax is -29.4 dB. No filtering preprocessing has been applied to the measured data. MTD-3 with the short pulse duration of 650 ps is called System-1 compared with the other one is System-2. The time and frequency representations of the pulses are depicted in Figure 4.

The characteristic features of the pulse signals are given in Table 1.

Table 1. *Data sets used in the experiments.*

Object	Dataset	Metallic content	Number of B-scan
Surrogate M14	Set-1	LM	60
Surrogate TS50	Set-1	LM	40
Surrogate VS50	Set-1	M	60
Surrogate PMN	Set-1	M	40
Surrogate PMD	Set-1	M	20
Coke can	Set-1	HM	60
Glass bottle	Set-1	NM	60
Plastic bottle	Set-1	NM	40
TOTAL	**Set-1**		**380**
Surrogate	Set-2	NM	40
Oil bin	Set-2	HM	60
Metal disk	Set-2	HM	40
Plastic disk	Set-2	NM	40
TOTAL	**Set-2**		**180**

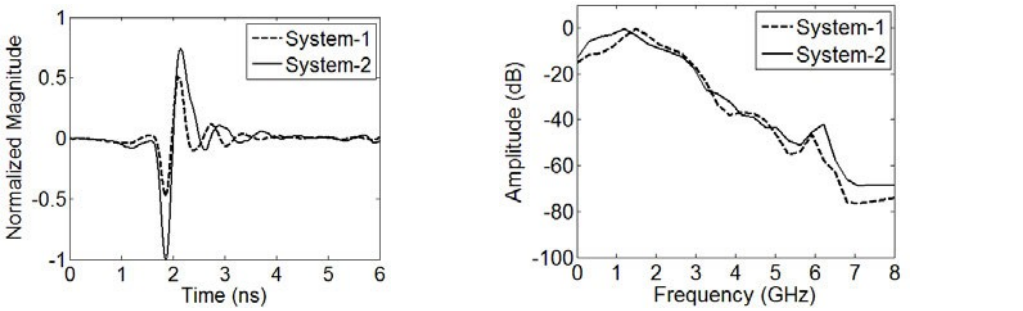

a) Time-domain representation of the pulses b) Frequency-domain representation of the pulses

Figure 4. *The short and the long pulses with the durations of 650 ps (System-1) and 870 ps (System-2), respectively.*

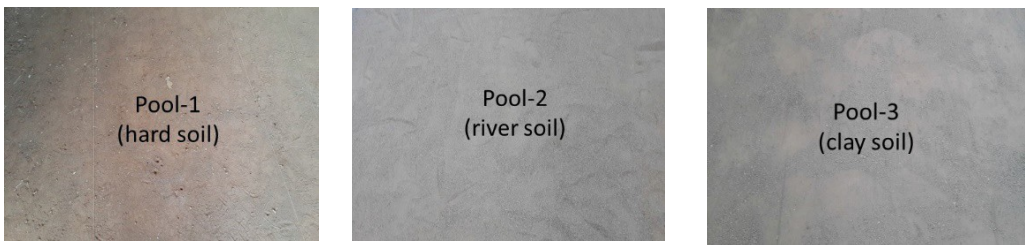

Figure 5: *Test pools*

3. METHODOLOGY

A representation of buried object identification scenario and sample sensor data are given in Figure 5. The coordinate system and buried object position are also shown in Figure 5(a). A sample B-scan image is given in Figure 5(b) which is reconstructed by horizontal concatenation of A-scan signals given in Figure 5(c). In this figure, $a0(z)$ represents the A-scan data acquired at position $y = 0$ and so on, where z is the depth index. Metallic density function of the object is also provided in Figure 5(d). Figure 5(b) and (d) are samples from real data recorded on a buried VS50 mine simulant.

$a_y(z)$: A-scan data (column vector) acquired at position y.
$B(y,z)$: Reconstructed GPR B-scan data (matrix) by concatenating sequential A-scans L: Length of A-scan signal
N: Number of A-scan signals in B-scan data

In this study, we use N = 240 A-scans to construct B-scan data. Each A-scan data contains L = 256 samples. The sensor data for the detected objects are first divided into three groups according to their metal density function, using Metal Detector (MD). Within each group, features are extracted from MTD-3 GP R responses, and landmine/clutter discrimination is achieved using a k-NN classifier.

3.1. Initial grouping

MTD-3 Mine Detector transmits an electromagnetic field that induces eddy currents in metallic object surfaces that are in the penetration range of the sensor. When the transmitted electro- magnetic field is abruptly turned off, eddy currents inside the targets produce a secondary magnetic field that is measured by the sensor. The strength of the measured signal primarily depends on the depth and the metallic content of the target. Based on the strength of the metallic density function, we pre-classify the objects into three classes using two thresholds.

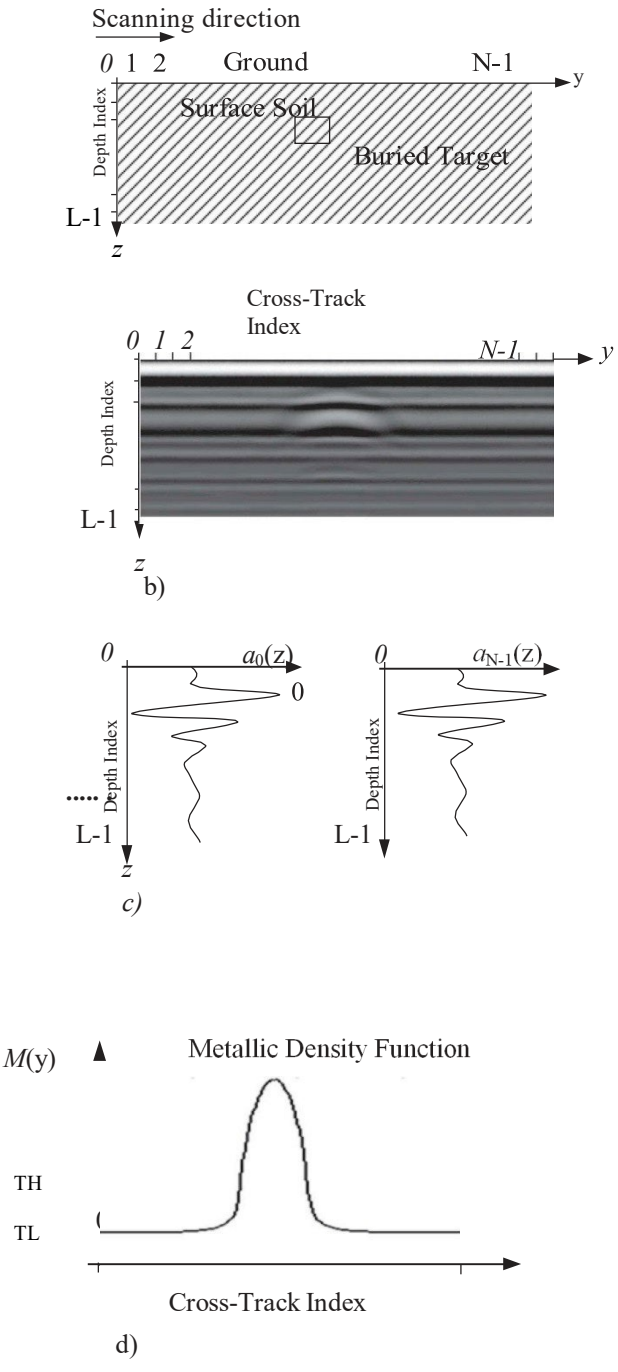

Figure 6. *Buried object identification scenario and sensor data. (a) Coordinate system and buried target representation. (b) Sample B-scan image – B(y,z) (A-scan signal intensities are inserted in each column of B-scan image). (c) Sample A-scan signals which are collected along the scanning directiony. (d) Metallic density channel of metal detector for a sample high metallic target.*

TL and TH. Denoting the maximum value of metallic density function for a specific target as *Mmax*, the target is classified as high metallic if *Mmax*>TH, low metallic if TL<*Mmax*<TH, or non-metallic if *Mmax*<TL. For example, the target corresponding to the sample EMI response in Figure 5(d) is labelled as a high metallic object. Conventionally, antitank (AT) mines are buried deeper than anti-personnel (AP) mines. Keeping this in mind, we set the thresholds such that burial depth of AT and AP mines is assumed to be around 5–50 cm.

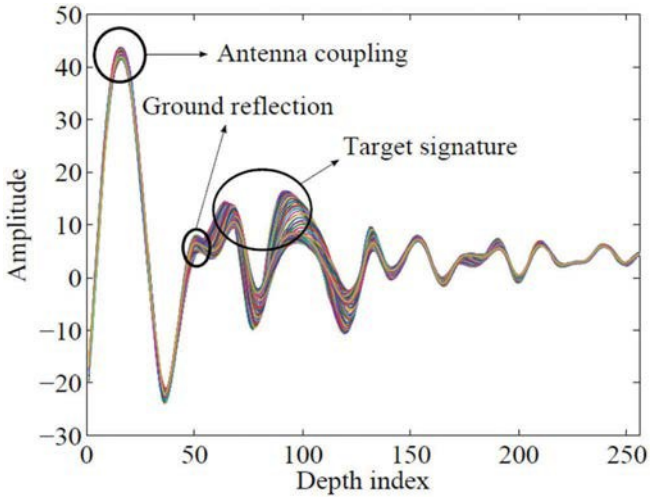

Figure 7. *A-scans overlaid on top of each other for sample MTD-3 GPR data.*

3.2. Feature extraction

Features are extracted using MTD-3 GPR responses of the buried objects. Using these features, classification is performed within each group. We propose that the scatter of the peaks among subsequent A-scans is a discriminant characteristic of the target. Remainder of this section will be explained on the sample B-scan given in Figure 5(b). This B-scan is recorded from a high metallic object buried at 10 cm under the ground surface.

In Figure 7, A-scans corresponding to the B-scan in Figure 5(b) are overlaid on top of each other with different colours. Antenna coupling, ground reflection and mine signature are marked on the plot. There are also some peaks deeper into the ground (higher depth indices), which arise due to the ringing effect in the detector hardware. The feature extraction step depends on the variations of the peak locations along the depth axis *z* "Figure 5(c)".

The hyperbolic structure in the B-scan implies that the peaks corresponding to the target signature will exhibit location variations along *y-z* plane. We keep the detector height is approximately constant, i.e., the operator sweeps the detector roughly at a constant height above the ground surface. The peak corresponding to ground reflection is not reveal a considerable variation along the depth axis. Ringing noise appears as nearly horizontal components in B-scans, which can be observed in Figure 5(b). This entails that the peaks arising from ringing noise will have negligible variation along the depth axis. Shortly, the most variant peaks along the depth axis will be the ones corresponding to the target signature.

3.3. The peaks Location

In the first step, a moving-average filter with length of 5 is applied to each A-scan signal to prevent undesired peaks caused by noise.

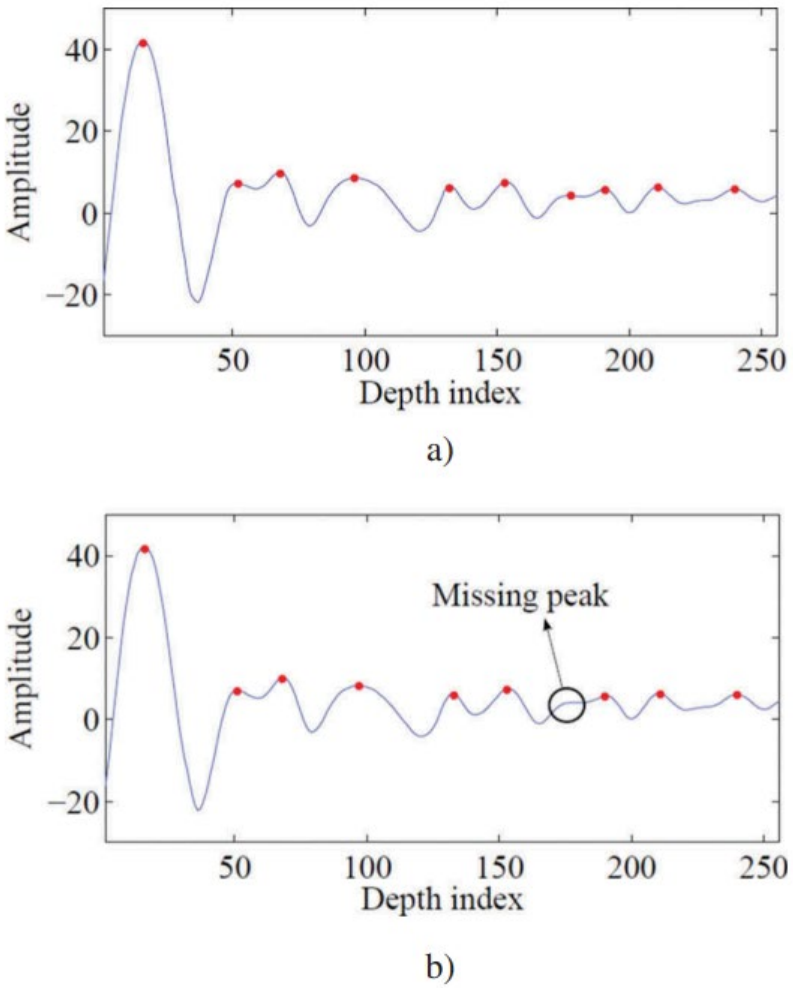

Figure 8 : *Explanation of missing peak phenomenon. (a) Sample A scan signal with 10 peaks. (b) Next A-scan signal following the one above, where one of the peaks is lost.*

To find the scatter of the peaks, we first marked the peak locations. We adopt a light-weight approach for computational efficiency. For a given A-scan, if a point has a larger amplitude than its immediate spatial neighbours, the point is said to be a peak point.

3.3.1. Grouping the peaks

Peaks on each subsequent A-scan should be grouped to find the scatter of each peak. For this purpose, spatial proximity to the peaks in the former A-scans within a window is considered, and the peaks that are close to each other among subsequent A-scans are said to be in the same group. The size of this window is important, it cannot be made too small as some peaks might disappear in certain A-scans due to noise. It cannot be made arbitrarily large either, as different peaks may overlap in the presence and absence of a buried object. Figure 3 demonstrates the missing peak phenomenon in consecutive A-scans. In this figure, peaks that could be located are marked with dots, and the missing peak is marked with a circle.

Evidently, the number of missing peaks also depends on how the peaks are located. In this study, we chose to locate peaks with a low-cost technique and solved the resulting imperfections afterwards. To compensate for missing and overlapping peaks, the peak groups whose mean depth indices are too close to each other are merged after all A-scans in the B-scan are processed. This is especially useful for AT mines, where the peak corre- sponding to the strong hyperbolic structure dominates the other peaks as the detector is swept over the mine. In Figure 9, the result of peak grouping is demonstrated for the given sample B-scan data, where each distinct peak group is shown with a different colour.

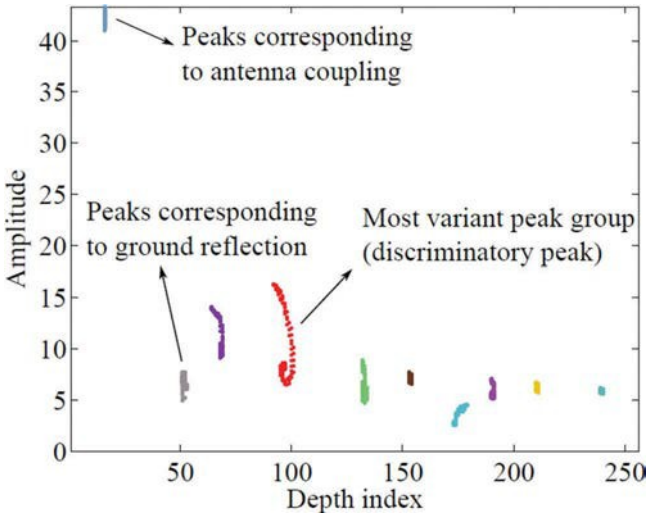

Figure 9. *Scattering of grouped peaks among subsequent A-scans.*

3.3.2. Finding the discriminatory peak

It is observed that a target signature may affect one or two peaks depending on the size and the burial depth of the object. However, as the feature vector must have the same number of elements for each buried object, scatter of a single peak group is used to characterize the object. This peak group is selected as the one which has the greatest variance along the depth axis.

3.3.3. Extracting relevant information from the peak scatter

As discussed before, we propose that the scatter of the most variant peak is an identifying characteristic of the buried object. To extract relevant information from the peak scatter that has the same dimensionality across B-scans to facilitate compar- isons, principal component analysis (PCA) is used. PCA finds the most meaningful basis to re-express a data set, which will reveal the hidden structure of the process.

We observed that an amplitude interval that is compar- able to the average variance of the peak scatter along the depth index works successfully for each type of buried object. Fals alarm rate is given at Figure 10.

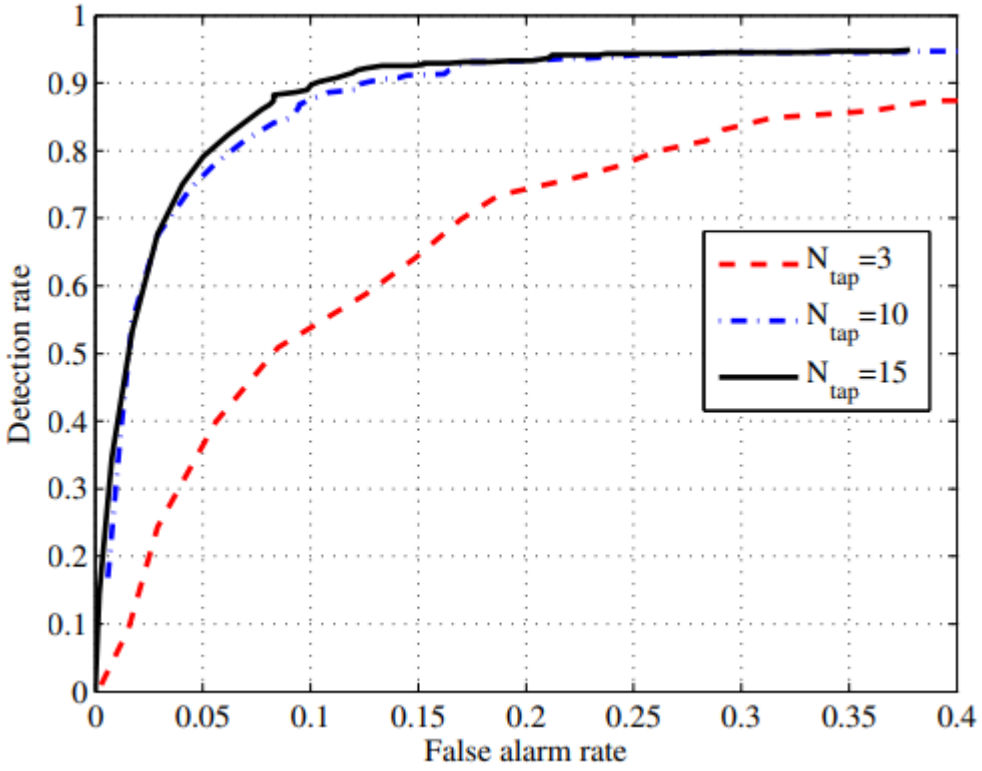

Figure 10. Falls *alarm rate of MTD-3.*

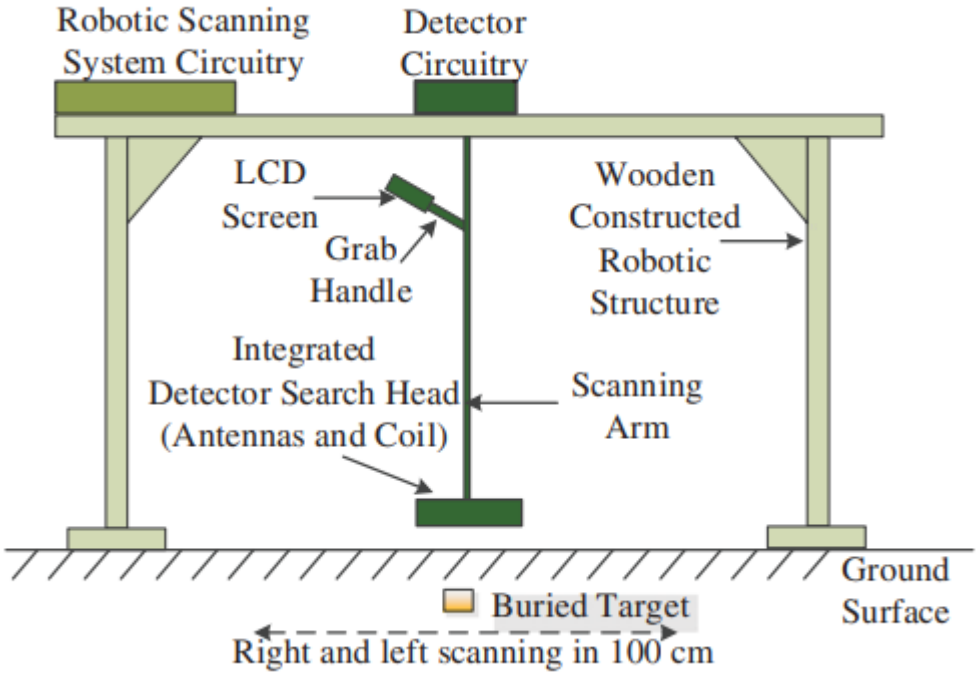

Figure 11. *Portable scanning system and data collection scenario.*

3.4. *Final classification*

After the initial grouping of the buried object according to its metal content, its MT D- 3 GPR features are compared to the other objects' features within the same metallic group using k-nearest neighbour (k-NN) algorithm. k-NN is an instance-based learning algorithm where new samples are classified by a majority vote of its neighbours in the training set. We selected to use the Euclidean distance as the distance function between the feature vectors. Simple unweighted voting is used as the decision function. Training set is defined as the set of feature vectors corresponding to all B-scans except the one which is being classified (leave-one-out technique).

4. *EXPERIMENTAL RESULTS*

In this section, identification results of the proposed method are presented. An illustra- tion of our experimental setup is given in Figure 9. MT D - 3 GPR antenna and metal detector coil have been integrated into a single case. Therefore, both GPR and MD data are collected simultaneously. Scanning velocity of the wooden-constructed robotic system is 20 cm/sec. Tests are performed at three different controlled terrains with different soil types and burial depths. Dielectric constants and conductivity values of the soil types are summarized in Table 2. Actually, dielectric constant of a material varies with frequency. For simplicity, an average value is provided for each soil type. Averaging is performed between 600 MHz and 2.2 GHz.

The data set is obtained by using the dual sensor detector MTD-3. The system operates on two main modes, detection and identification. When a detection alarm occurred during detection scanning, another scan is performed with approximately 0.2m/sec scanning speed by centring the suspicious region within 1 m distance. The antenna bandwidth of GPR sensor is approximately 1.5 GHz. The following information is given to the operator instantaneously on LCD screen of the system.

Table 2. *Electromagnetic properties of soil types.*

Soil type	Dielectric constant	Conductivity (S/m)
Type 1	2.33	0.0030
Type 2	2.75	0.0008
Type 3	2.59	0.0012

Table 3. *Data set used in the experiments*

	Object name	Number of signatures
Non-metallic (Group 1)	Glass bottle	60
	DM11AT Mine simulant	40
	Rock	60
	VS1.6 Mine simulant	20
	Number of Group 1 signatures	180
Low metallic (Group 2)	Iron nail	40
	DM11AP Mine simulant	40
	M14 Mine simulant	60
	PMN Mine simulant	20
	TS50 Mine simulant	40
	VS50 Mine simulant	20
	Number of Group 2 signatures	220
High metallic (Group 3)	Soft drink can	20
	M15 Mine simulant	20
	M6A2 Mine simulant	60
	M7A2 Mine simulant	40
	PMD Mine simulant	20
	TM62M Mine simulant	20
	Oil bin	60
	Number of Group 3 signatures	240
Number of total signatures		640

- Inspected region cross-track GPR image
- Reflected energy function for GPR
- Detection information for GPR
- Metal density function for EMI
- Detection information for EMI

The total number of object signatures (B-scans) in the data set is 640. The number of distinct targets is 17. From each target, B-scans are recorded in four scanning directions (right, left, up, down). The detector search head height from ground surface is approxi- mately 5 cm. Antipersonnel and antitank mine simulants and some other objects that are commonly encountered under the ground are used in the tests. Table 2 tabulates the types of the buried objects, metallic content of each object and the corresponding number of object signatures.

Content and size of mine simulants have very similar characteristics to the real mines. As these values follow the standards, they are not given here. We only give size

Table 4. *Burial depths of the targets (in cm).*

Object group	Burial depths (cm)
Group 1	7, 9, 10, 20, 50
Group 2	5, 7, 10, 20, 40,50
Group 3	10, 25, 50, 60,100

Table 5. Identification results of the proposed method (after initial grouping into non-metallic, low metallic and high metallic groups).

Object grouping	Number of false alarms (mis-identification)	Number of signatures	Identification rate (%)
Non-metallic (Group 1)	0	180	100.00
Low metallic (Group 2)	9	220	95.91
High metallic (Group 3)	3	240	96.25
Overall	12	640	98.13

information of clutter objects. Buried rock's longest edge is 8 cm. The glass bottle has a height of 18 cm and the radius of its largest cross section is 4 cm. Length of the iron nail is 6 cm. Buried soft drink can is a crushed cylindrical coke can, diameter of which is 6.5 cm and height of which is roughly 2 cm. The oil bin is a metallic rectangular prism-shaped object having a size of 12 × 20 × 3 cm. The burial depths of the objects are given in Table 4.

After the initial grouping step of buried object data according to metallic density function, size of the window within which peaks are searched and grouped is taken to be 10 A-scans.

Landmine/clutter discrimination rates for each group of objects are given in Table 4. Overall, 628 B-scans out of 640 were correctly identified, giving an average identification rate of 98.13% for the proposed method (false alarm definition involves both misidentified mines and misidentified other objects).

To assess the impact of the initial grouping, we performed two additional experi- ments. The first one uses only metallic and non-metallic pre-classification according to metallic density channel, followed by the proposed peak scatter modelling-based

Table 6. *Identification results of the proposed method (after initial grouping into non-metallic and metallic groups).*

Object grouping	Number of false alarms (mis-identification)	Number of signatures	Identification rate (%)
Non-metallic (Group 1)	0	180	100.00
Metallic (Group 2 and Group 3)	12	460	97.39
Overall	12	640	98.13

Table 7. *Identification results of the proposed method (no initial grouping according to metal density).*

Object grouping	Number of false alarms (mis-identification)	Number of signatures	Identification rate (%)
No grouping (All signatures)	27	640	95.78
Overall	**27**	**640**	**95.78**

Table 8. *Effect of training data size on identification rate.*

	Training data size	20 %	40 %	60 %	80 %	Leave one out technique
Identification rates (%)	Non-metallic, low metallic and high metallic initial grouping (The proposed method)	92.18	96.35	97.26	97.65	98.13
	Non-metallic and metallic initial grouping	88.08	95.05	96.87	97.65	98.13
	Without initial grouping	84.77	88.28	93.36	94.53	95.78

MBI SAVUNMA ve ALANI ARAMA
TEKNOLOJİLERİ A.Ş
Reşitpaşa Mah. Katar Cad. Teknokent
Arı 1 Sit. No: 2/5-19 Sarıyer / İSTANBUL
Ticaret Sicil No: 110700-5
Sarıyer V.D. 6131213532

Berkay Turgay
Engineer
R&D Director
MBI Savunma Ve Alan Tarama, Maslak, Istanbul, Turkey.